

Design and Finite Element simulation of Tracking System for Parabolic Trough Solar Collector

Mohammed Younus Ammar Alhamd

Department of Mechanical Engineering, University of Mosul, Nineveh, Iraq

Ammar Younis Ibrahim Alrawy

Department of Mechanical Engineering, University of Mosul, Nineveh, Iraq

Ziad Shakeeb Alsarraf

Department of Mechanical Engineering, University of Mosul, Nineveh

Abstract

With the development of solar energy harvesting technology, it has become necessary to have total control over the collection of sunlight energy through solar complexes with a tracking system that helps to obtain the largest amount of incoming sunlight. Metal and teeth to face mechanical stresses and the effect of heat on them, where the two systems were taken and analyzed, and the weaknesses and strengths of these mechanical parts were known. Through the results that were extracted, it was shown the ability of these mechanical parts to bear stress and the effect of heat on them, as it took three temperatures that the solar collector can pass through, and that the most deformation and the weakest ability of the gear was at the temperature of 40 degrees Celsius.

Keywords: tracking system, SOLIDWORKS, dual axis, safety factor, ANSYS, solar energy, solar collector

1. Introduction

Sun worldwide situating structures include robotized sheets that follow sun-controlled spreads to achieve an ideal point between radiations delivered from the sun and the daylight-based charger. The justification for this proposition study is to plan and copy two slew drives that turn the sunlight-based charger a vertical way and equally [1]. An examination of a photovoltaic global positioning framework is directed, to concentrate on its productivity dependent on the consequences of a particular power plant. A solitary axis system is investigated, considering diverse lists to better characterize the general framework execution. Exploratory data have been gathered by an on location checking framework over a time of one year [2]. Sunlight based increase on a sun powered charger is identified with its direction - following the sun about the east-west center was most really dreadful to help the energy variety of daylight fueled chargers, and following the sun about the south-north center point was great. Results in like manner showed that the extent of yearly collectible radiation on level South-Orth sun-center followed daylight based chargers was reasonable to be utilized in districts with lower topographical scopes [3]. A functioning single pivot sun-oriented tracker can be mounted on a divider to give adaptability to various climate conditions and inclination for various clients. Sun oriented irradiance is dictated by sensors that are situated on the outer layer of the photovoltaic (PV) board. The effectiveness over the proper sunlight-based charger, the power created and the kinds of PV frameworks not set in stone before genuine execution [4]. A versatile sunlight based global positioning framework is executed to build energy age of the photovoltaic (PV) boards. The information got by the information procurement cards is shipped off a PC by means of Universal Serial Bus (USB) convention. This information is checked through the interface coded in PC and also recorded in the data set [5]. Sun based energy addresses a spotless and reasonable energy asset for some nations all throughout the planet. A sun powered global positioning framework can essentially work on the assortment of sunlight-based energy. The current half breed STS gives a uniform Performance proportion of about 97% for a 60 W PV board from dawn to dusk [6]. The global positioning framework is utilized for working on the proficiency of a photovoltaic board. It targets diminishing the rakish field of the day-by-day movement and the quantity of activating tasks. The energy utilization for achieving the following is controlled by mimicking dynamic conduct of the sun powered tracker [7]. A working sun tracker for sun-based streetlight got together with photoelectric after mode and time delicate after mode assistant was proposed. An authentic model named Available Energy Absorption Model was attempted to focus on the energy adequacy. The ordinary worth of energy adequacy in a year is 36% [8]. Ideal plan of a framework fit for proceeding to lead the sunlight-based charger to the ideal situation to guarantee maximum sunlight. An immediate transition and force control (DTC) is then applied to an enlistment engine (IM) which can develops the force needed to advance the area of the solar panel [9].

2. Methodology

The mechanical parts were designed through the global system iso in the Solid program, and the dimensions were given from these connections after adding the number of teeth, and the inner diameter of the gear, where different dimensions were used for the upper gear responsible for the movement of the solar collector vertically and the lower gear for the movement of the solar collector horizontally.



Figure (1): Solar collector with tracking system.

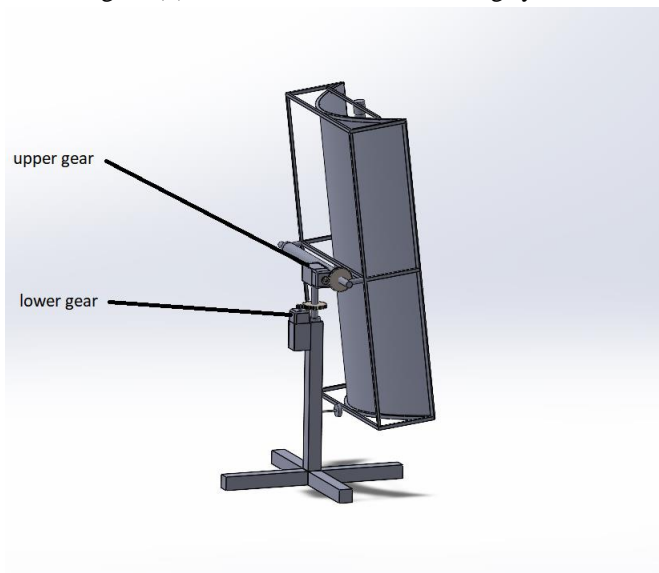


Figure (2): The locations of the gear.

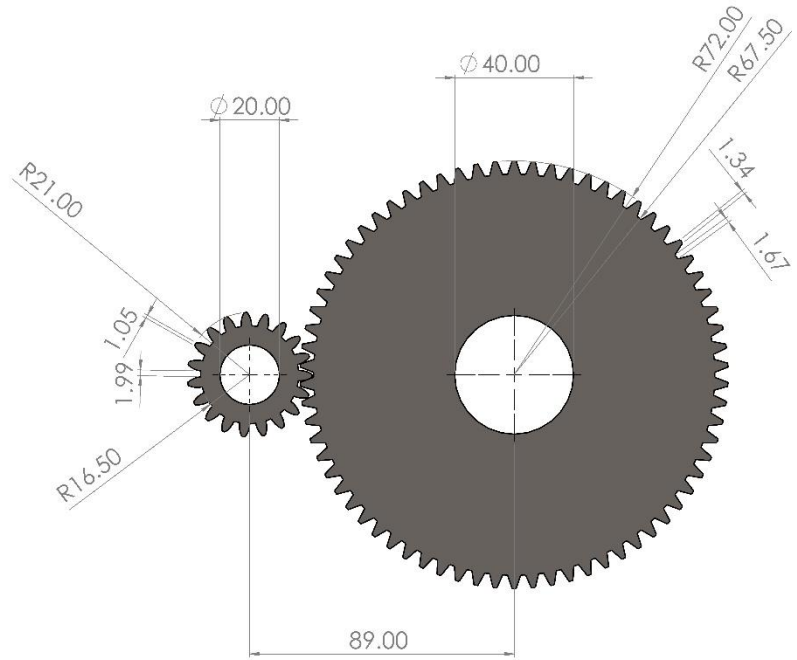


Figure (3): Dimensions of the upper gear in mm.

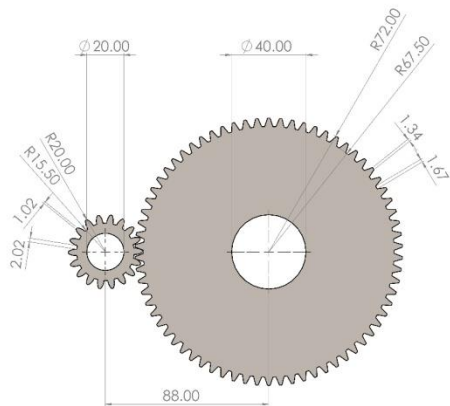


Figure (4): Dimensions of the lower gear in mm.

Two types of large gear were used, which have 70 teeth and 25.12 mm thickness, the upper small gear with 19 teeth and 26.12 mm thickness, and the lower small gear with 18 teeth and 24.1 mm thickness.

After the design process, it has to be entered into the ANSYS program to be simulated accurately. The mesh must be done accurately to give great reliability in the solution and get accurate results.

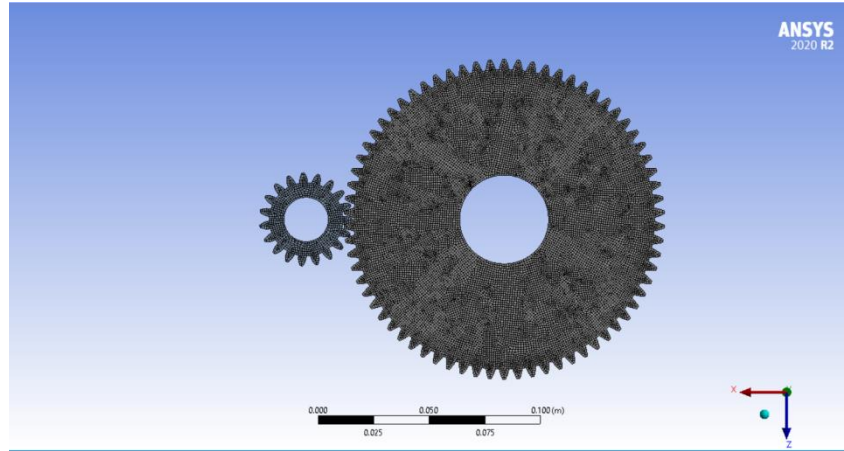


Figure (5): Mesh geometry.

Table (1): Mesh independency

case	node	element	deformation mm
1	632044	182663	0.035067
2	1021567	296346	0.016423
3	1336788	341296	0.014402
4	1651963	388542	0.014322

Through the number of the element 388542 shows the stability of the results and access to accurate results through this mesh.

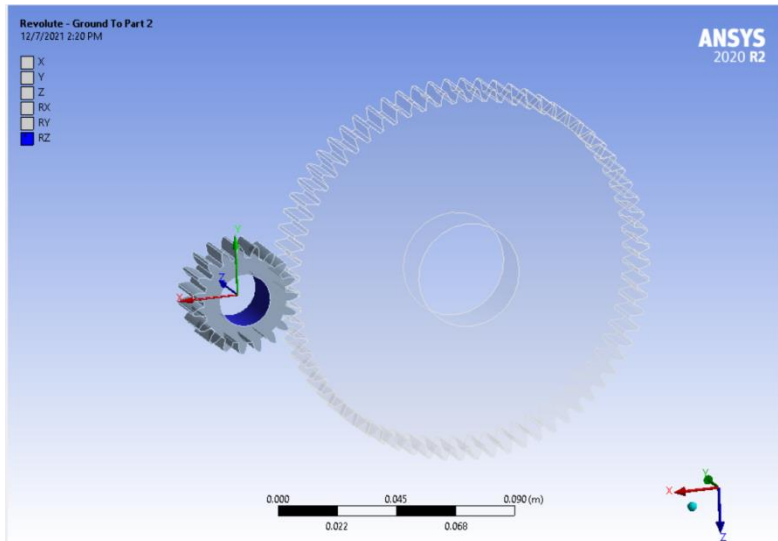


Figure (6): Small gear rotation.

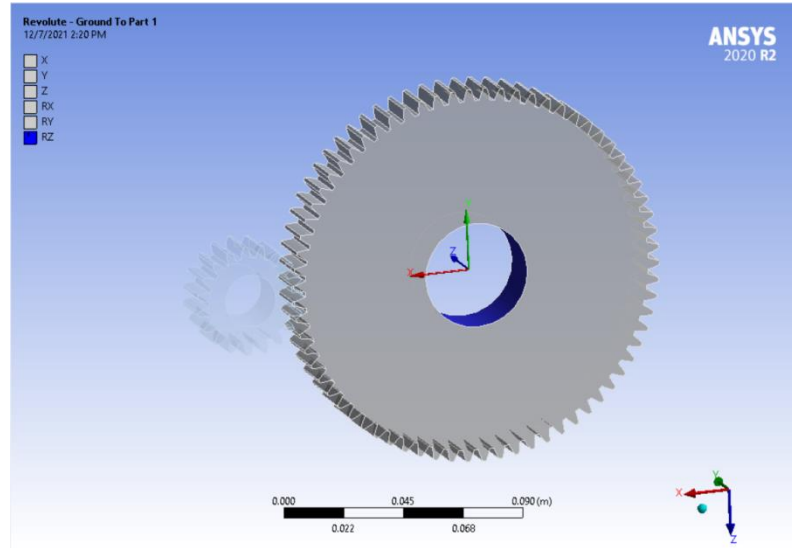


Figure (7): Big gear rotation.

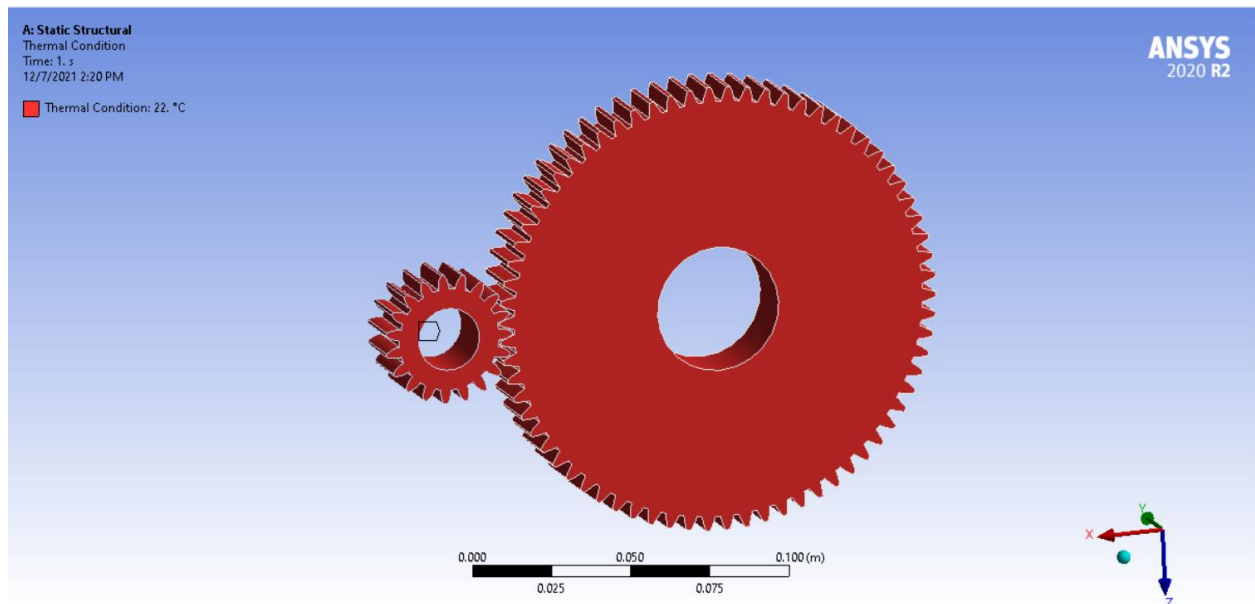


Figure (8): Thermal condition of gears.

Where three temperatures (22, 30 and 40) degrees Celsius were used to know the effect of the heat shed by the sun's rays on the mechanical stresses.

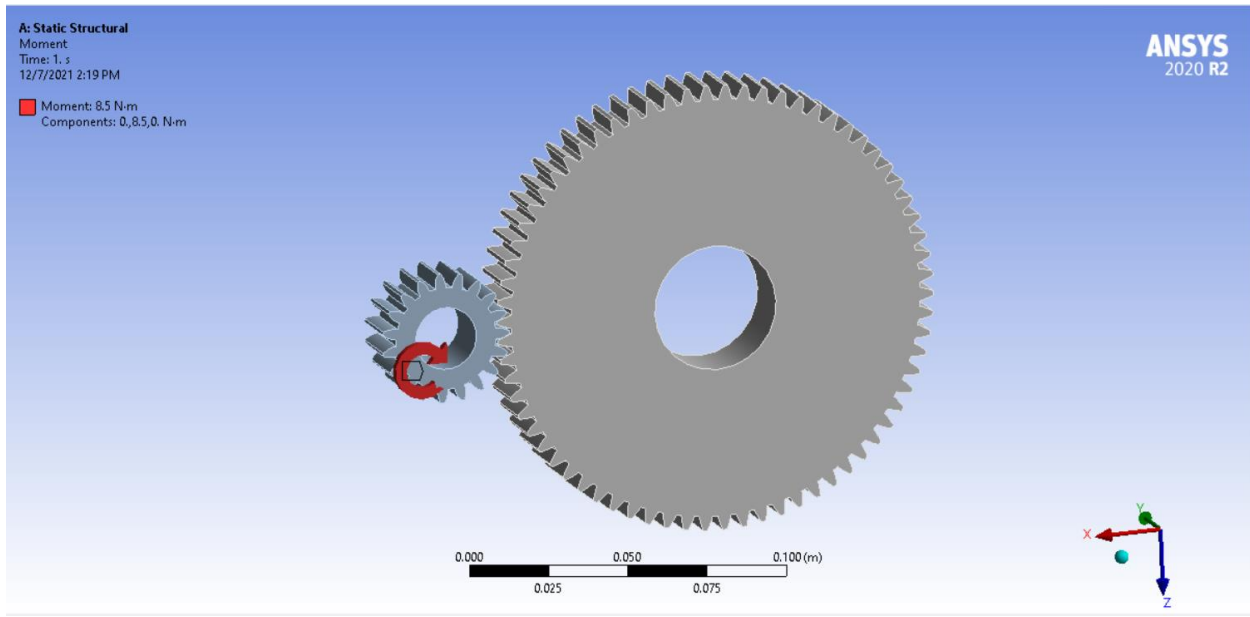


Figure (9): Moment applied on small gears.

Where a torque of 8.5N/m was used on the small gear, as this torque was taken from the step motor used in the tracking system.

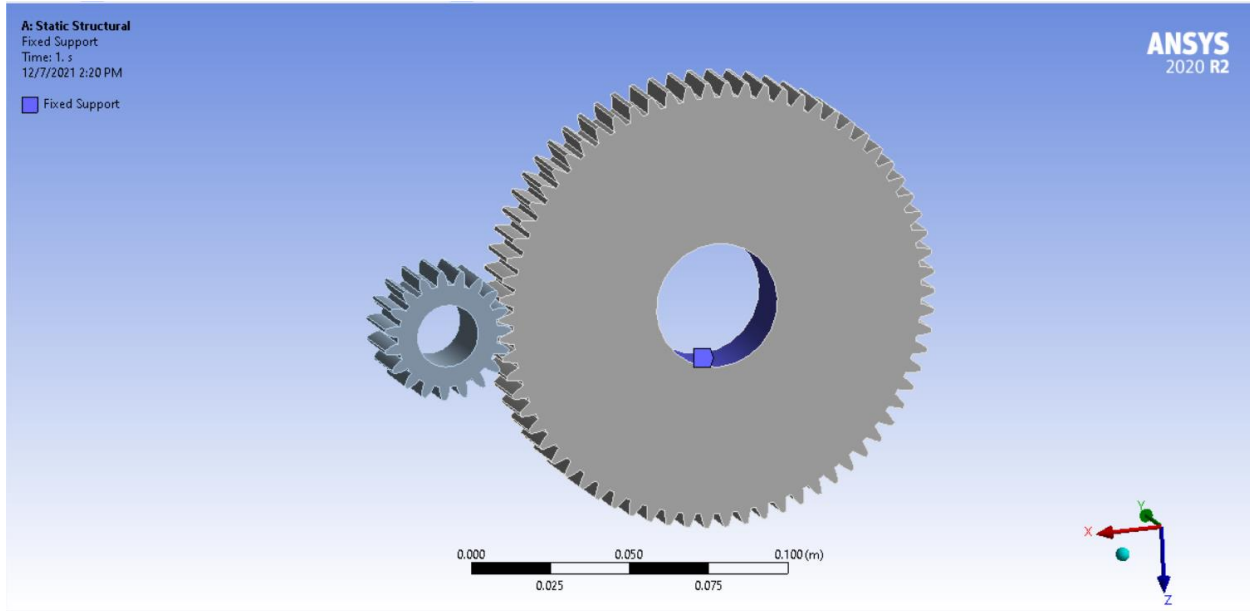


Figure (10): Fixed support on big gears.

The large gear axis has been installed to obtain the largest amount of stress that can be exposed to the insert through the step motor.

Where steel was used in the manufacture of gear and also in the simulation process with mechanical and thermal specifications.

Table (2): Material properties.

property	value	unit
density	7850	kg/m ³
coefficient of thermal expansion	0.000012	1/C
young's modulus	2E+11	Pa
poison's' ratio	0.3	
bulk modulus	1.6667E+11	Pa
shear modulus	76923000000	Pa
strength coefficient	920000000	Pa
strength exponent	-0.106	
ductility coefficient	0.213	
ductility exponent	-0.47	
cyclic strength coefficient	1000000000	Pa
cyclic strain Hardening exponent	0.2	
tensile yield strength	250000000	Pa
compressive yield strength	250000000	Pa
tensile ultimate strength	460000000	Pa
compressive ultimate strength	0	Pa

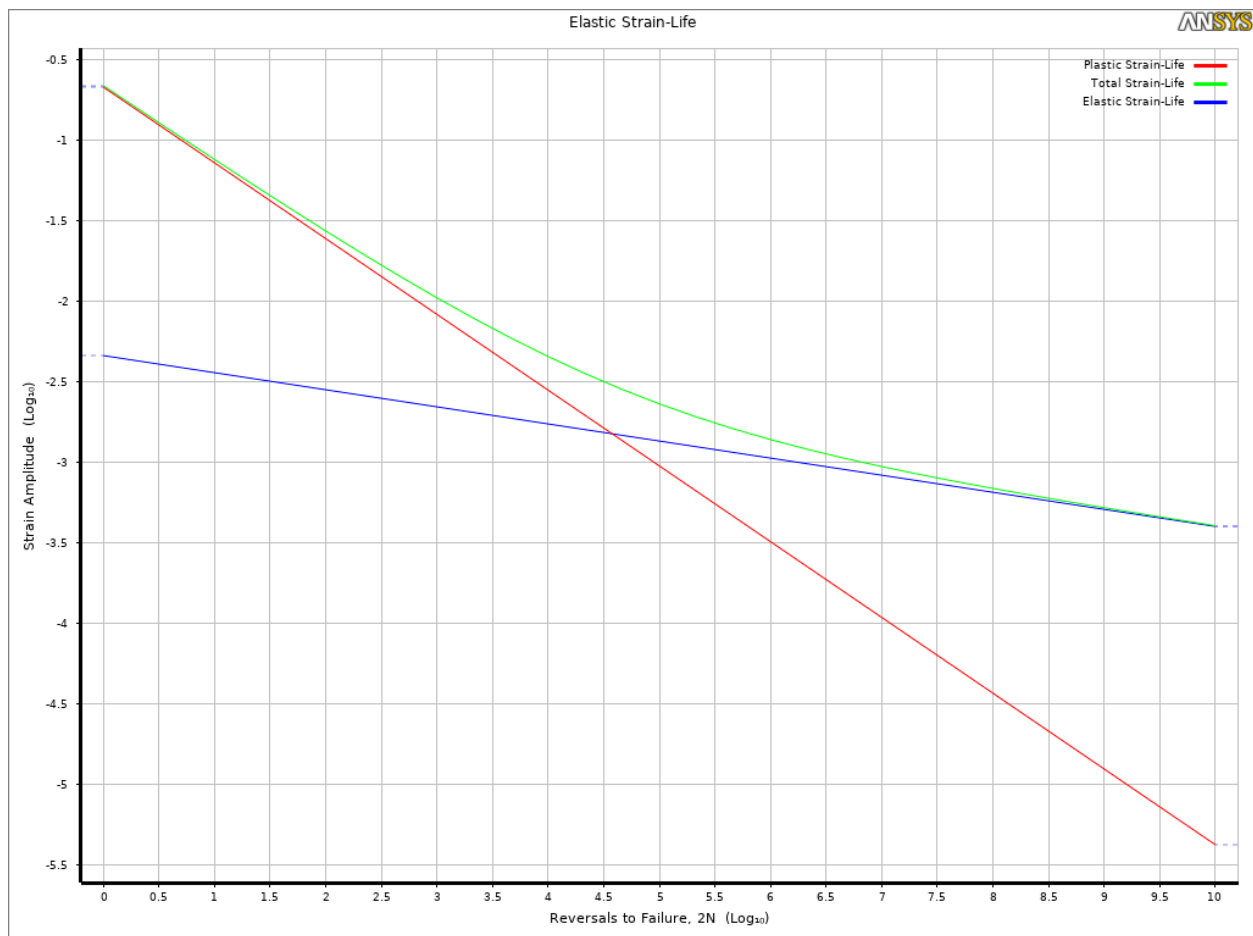


Figure (11): Strain amplitude.

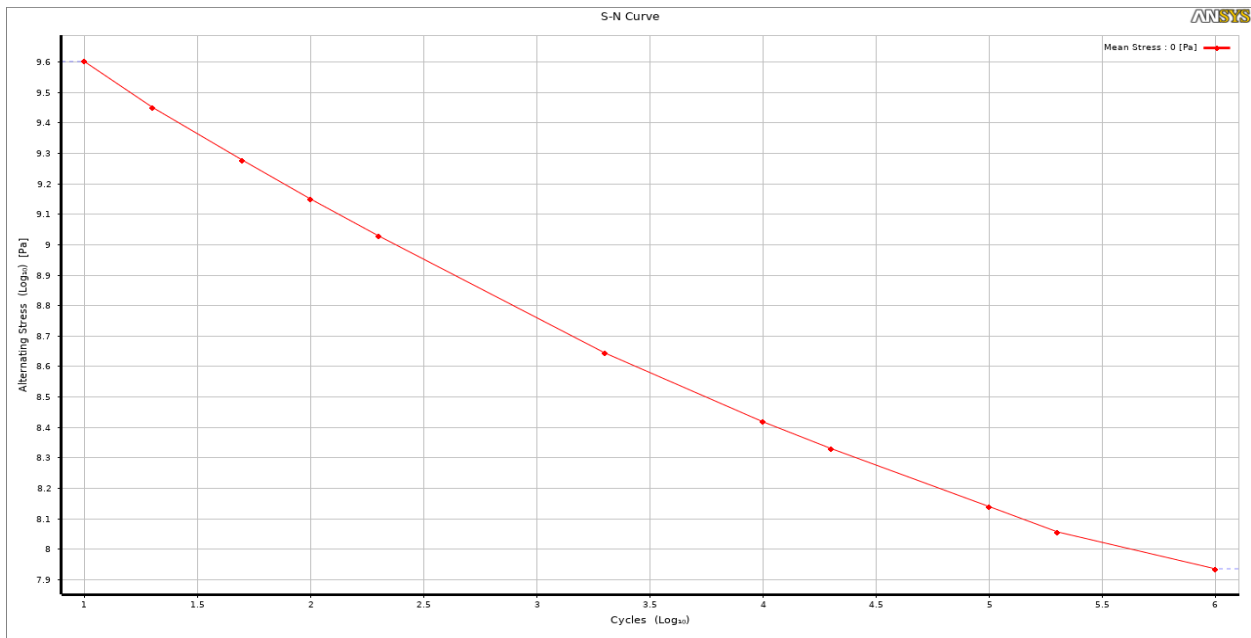


Figure (12): Alternating stress.

3. Governing equations

The general balance conditions for straight primary static investigation are:

$$[K]\{u\} = \{F\} \quad \dots \quad (1)$$

or

$$[K]\{u\} = \{F^a\} + \{F^r\} \quad \dots \quad (2)$$

where:

$$[K] = \sum_{m=1}^N [K_e] \quad \dots \quad (3)$$

$\{u\}$ = nodal dislodging vector

N = number of elements

$[K_e]$ = component solidness framework (depicted in Element Library) (may incorporate the component stress firmness grid (portrayed in Stress Stiffening))

$\{F^r\}$ = response load vector

$\{F^a\}$, the complete applied burden vector, is characterized by:

$$\{F^a\} = \{F^{nd}\} + \{F^{ac}\} + \sum_{m=1}^N (\{F_e^{th}\} + \{F_e^{pr}\}) \quad \dots \quad (4)$$

where:

$\{F^{nd}\}$ = applied nodal load vector

$\{F^{ac}\} = -[M]\{a_c\}$ = acceleration load vector

$$[M] = \sum_{m=1}^N [M_e] = \text{total mass matrix}$$

$[M_e]$ = "component mass grid (portrayed in Derivation of Structural Matrices)"

$\{a_c\}$ = all out speed increase vector (characterized in -(Acceleration Effect))

$\{F_e^{th}\}$ = component warm burden vector (portrayed in Derivation of Structural Matrices)

$\{F_e^{pr}\}$ = component pressure load vector (portrayed in Derivation of Structural Matrices)

To outline the heap vectors in Equation 2, consider a one component section model, stacked exclusively by its own weight, Applied and Reaction Load Vectors. Note that the lower applied gravity load is applied straightforwardly to the forced dislodging, and consequently causes no strain; all things considered, it adds to the response load vector similarly however much the upper applied gravity load. Additionally, if the solidness for a specific DOF is zero, any applied loads on that DOF are disregarded.

The general conditions for direct first request frameworks are as old as a straight primary static investigation, Equation 1 and Equation 2. $[K]$, however, is the all out coefficient lattice (e.g., the conductivity network in a warm examination) and $\{u\}$ is the nodal DOF esteems. $\{F^a\}$, the all out applied burden vector, is characterized by:

$$\{Q^a\} = \{Q^{nd}\} + \sum_{m=1}^N \{Q_e\} \quad \dots \quad (5)$$

Classification relates the terminology utilized in Derivation of Heat Flow Matrices and Derivation of Electromagnetic Matrices for warm, attractive and electrical examinations to Equation 2 and Equation 4, Nomendature of Coefficient Matrices for a more definite classification portrayal.

$\{u\}$	$\{F^{\text{nd}}\}$	$\{F_e\}$
Thermal $\{T\}$ temperature	$\{Q^{\text{nd}}\}$ heat flow generation convection	$\{Q_e\} + \{Q_e^g\} + \{Q_e^c\}$ heat flux heat

4. Results and discussion

Through the analysis and simulation of the gear responsible for the movement of the solar collector in the sequential system, three temperatures that the solar collector can pass through (22, 30 and 40) degrees Celsius were taken, and on them the results were taken mechanical stresses.

Comparison of upper and lower forging stresses at 20°C

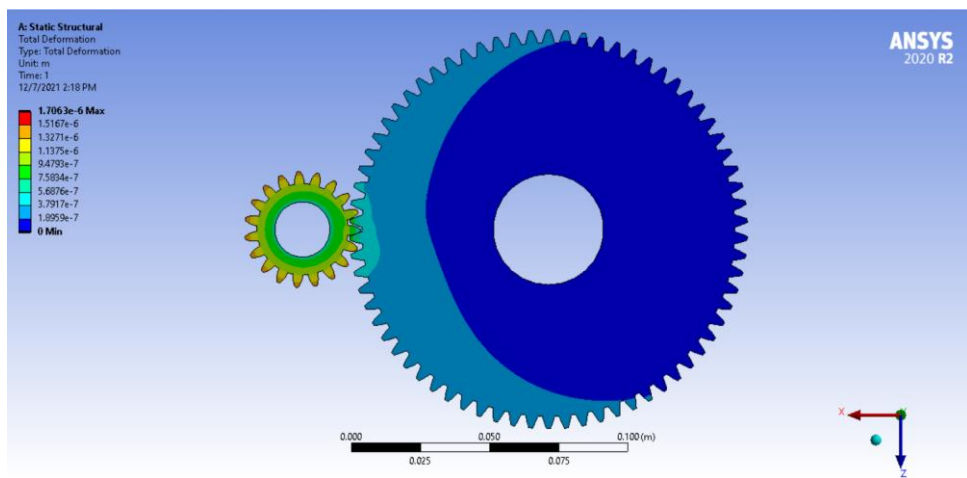


Figure (13): Deformation of upper gear.

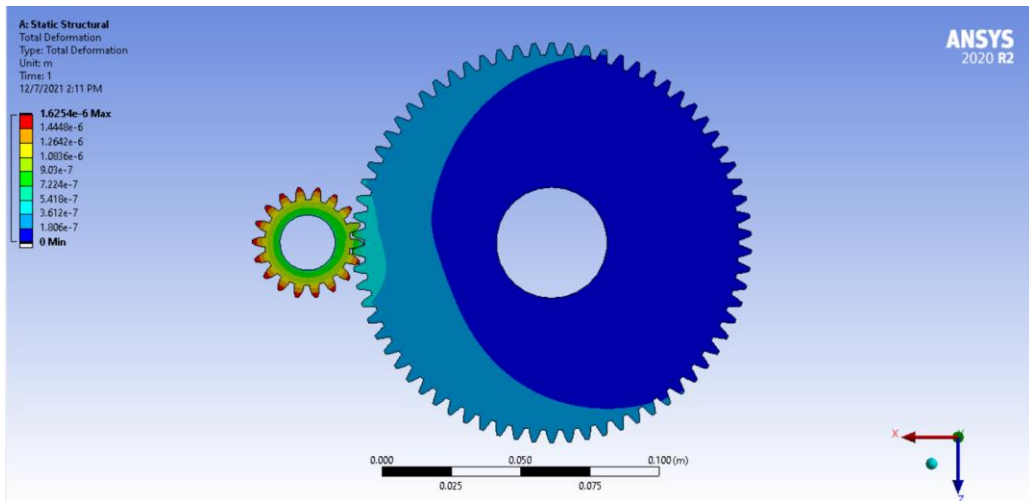


Figure (14): Deformation of lower gear.

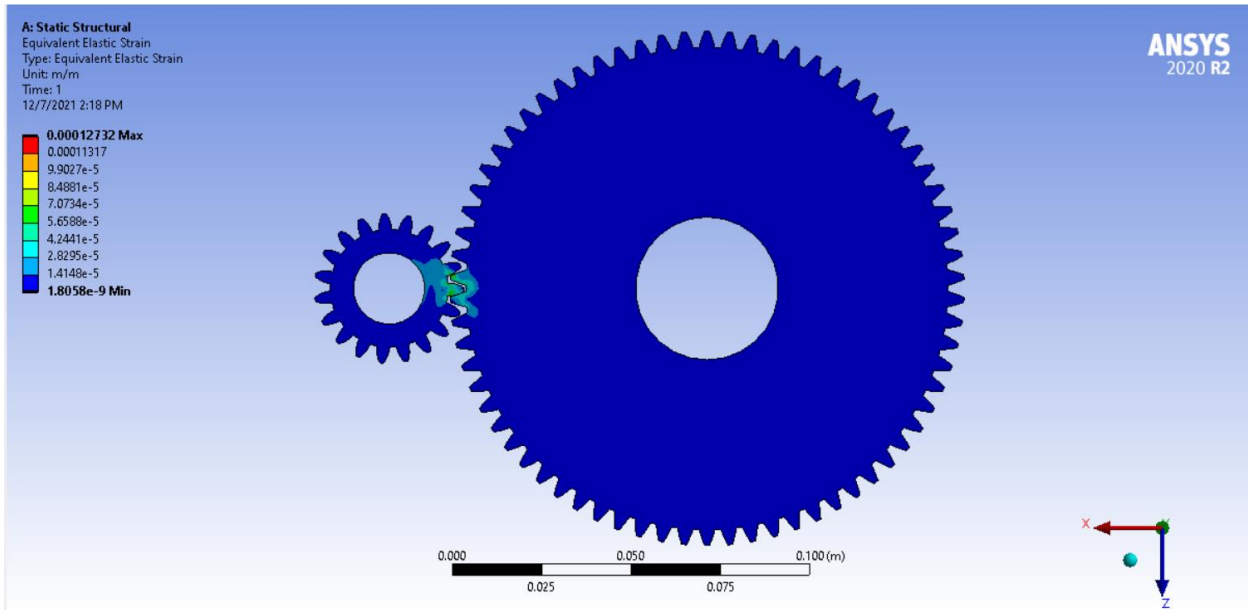


Figure (15): Equivalent elastic strain of upper gear.

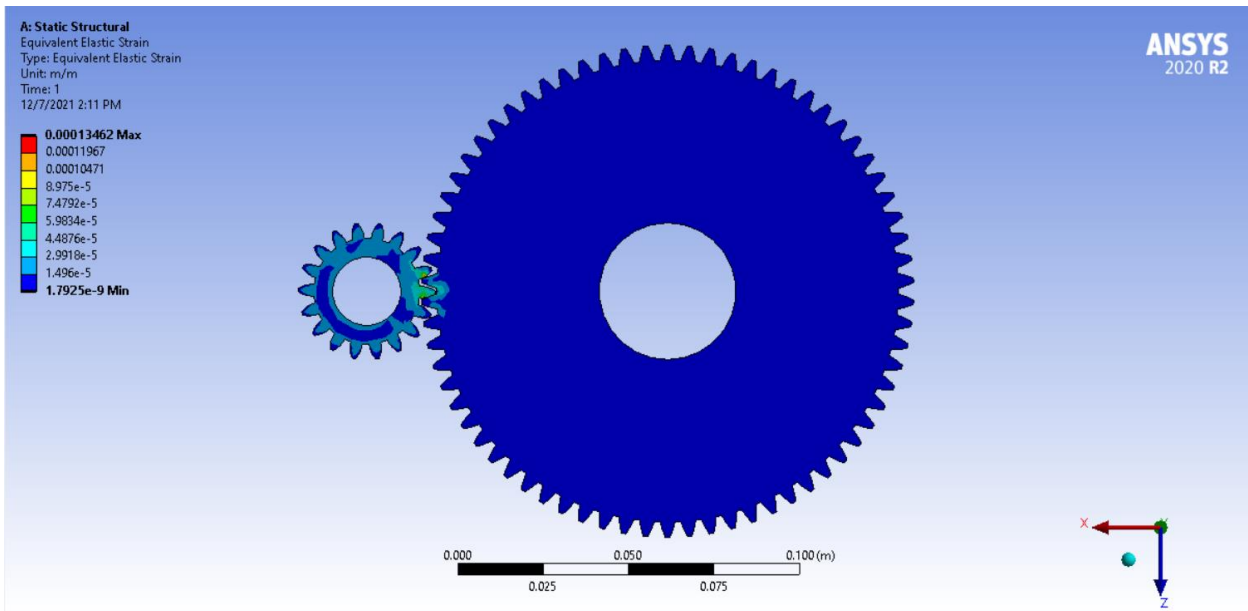


Figure (16): Equivalent elastic strain of lower gear.

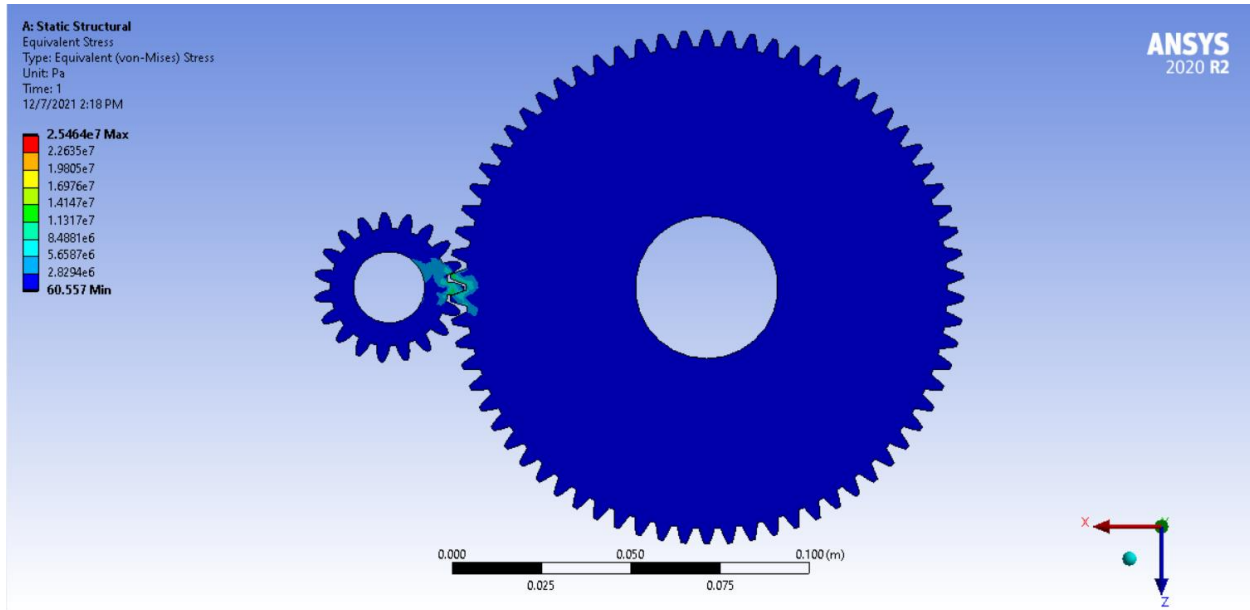


Figure (17): Equivalent stress of upper gear.

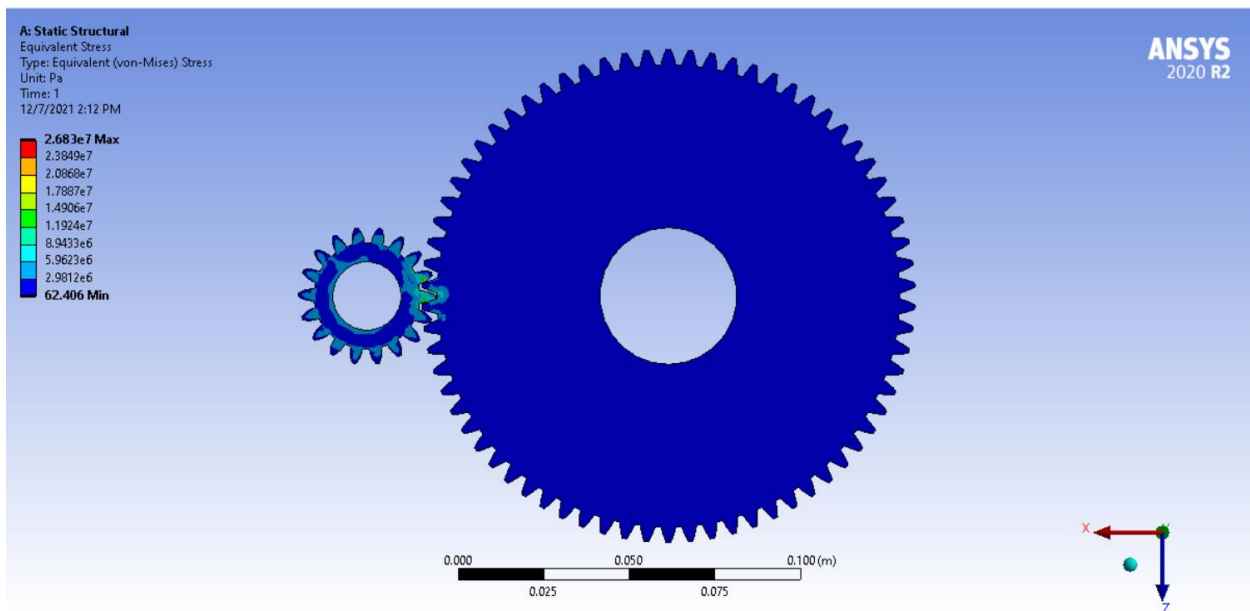


Figure (18): Equivalent stress of lower gear.

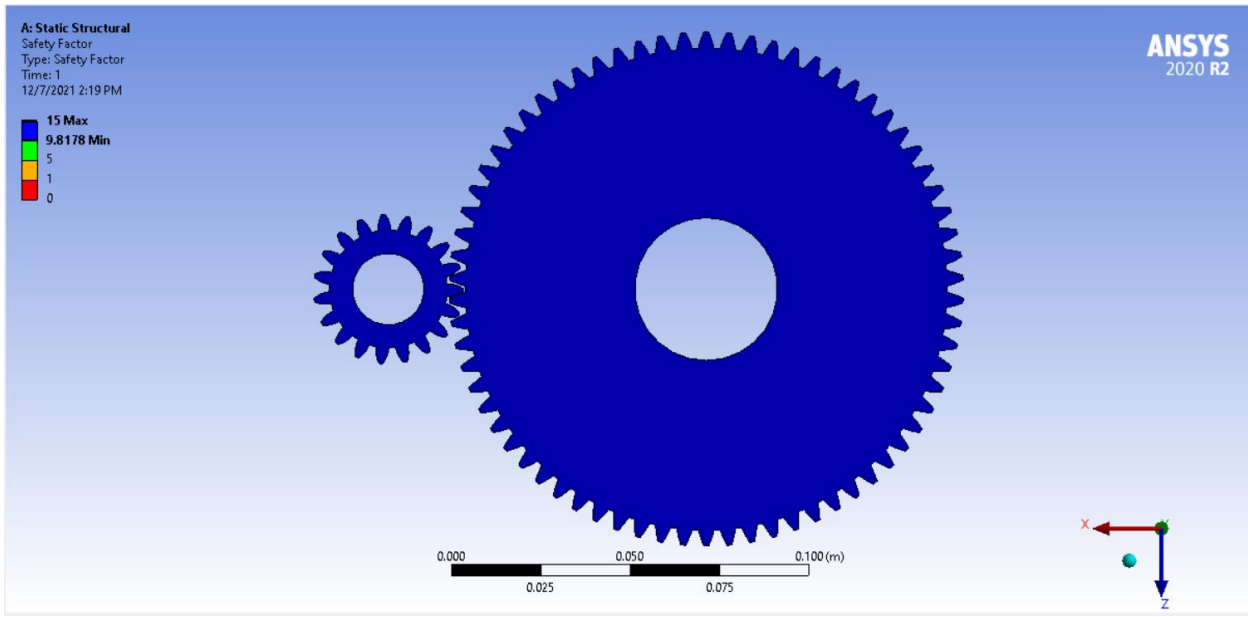


Figure (19): Safety factor of upper gear.

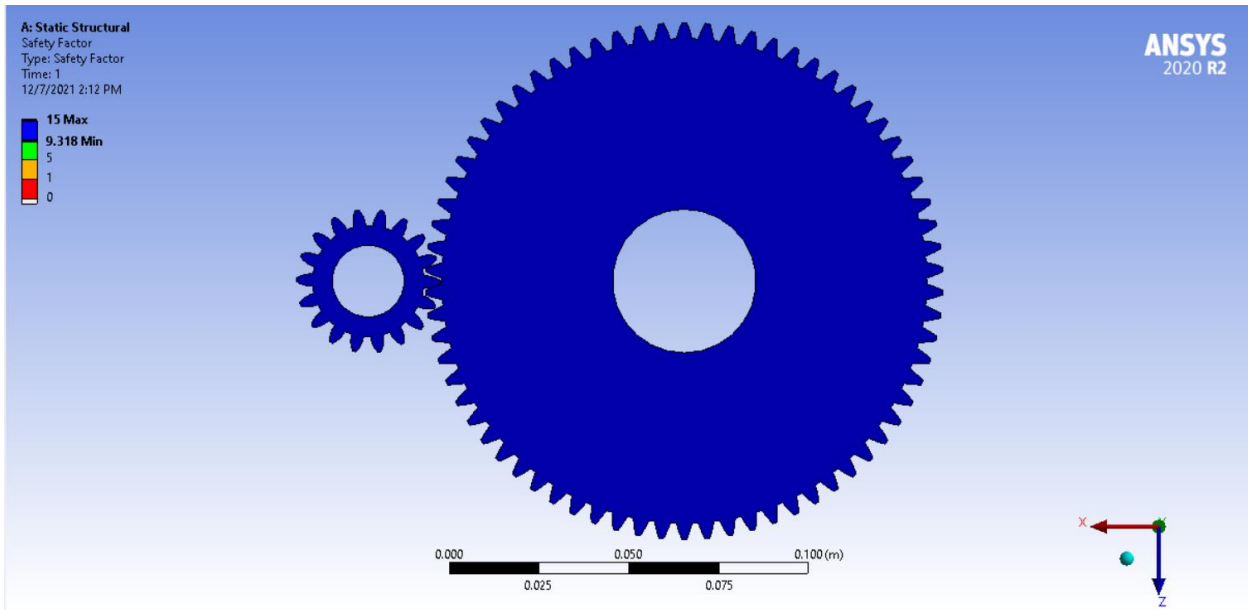
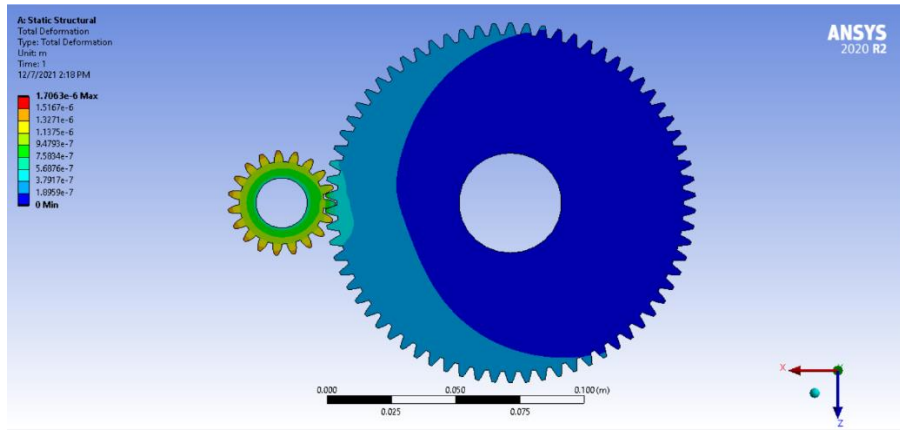


Figure (20): Safety factor of lower gear.

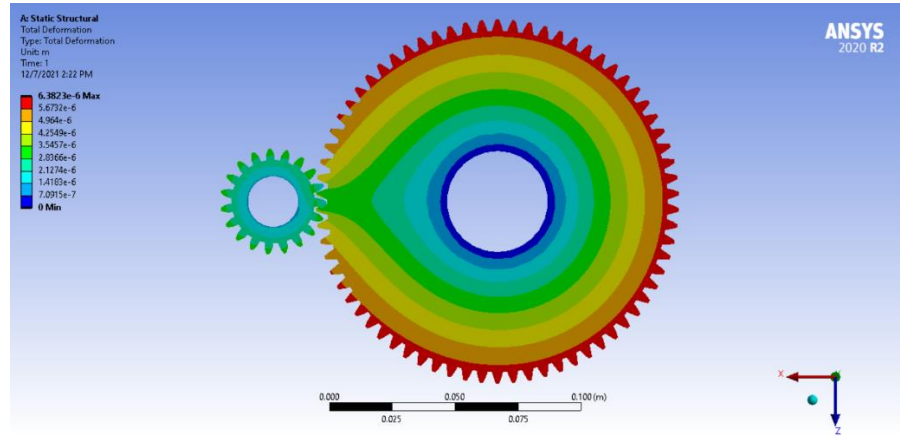
Through the previous results between the upper and lower gears, it was found that the amount of deformation in the upper gear is slightly more than the lower gear, where the maximum amount of deformation obtained by the upper gear was 0.000001706m, while the difference in the amount of strain shows that the lower gear is greater than the upper gear with a maximum value of 0.000134 m/m, as the stresses of the two types of bellows were in the interest of the lower keel, as it was greater by the amount of stress than the upper keel with a value of 26830000 pa, which is a great stress value in such cases, but in both cases it is clear by the value of the safety constant that both the upper and lower keel are in a great safety stage.

The effect of heat on mechanical stress

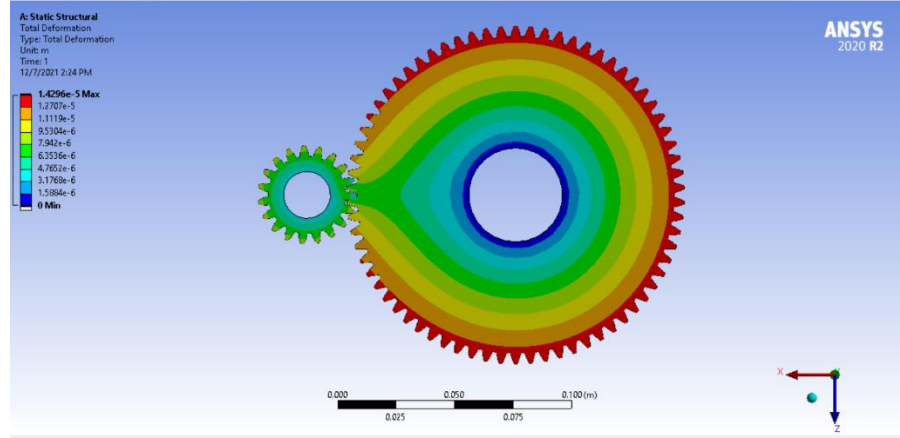
Where the effect of temperature differences and their effect on thermal stresses was investigated.



(a)



(b)



(c)

Figure (21): Deformation at. (a)22°C, (b)30°C, (c)40°C.

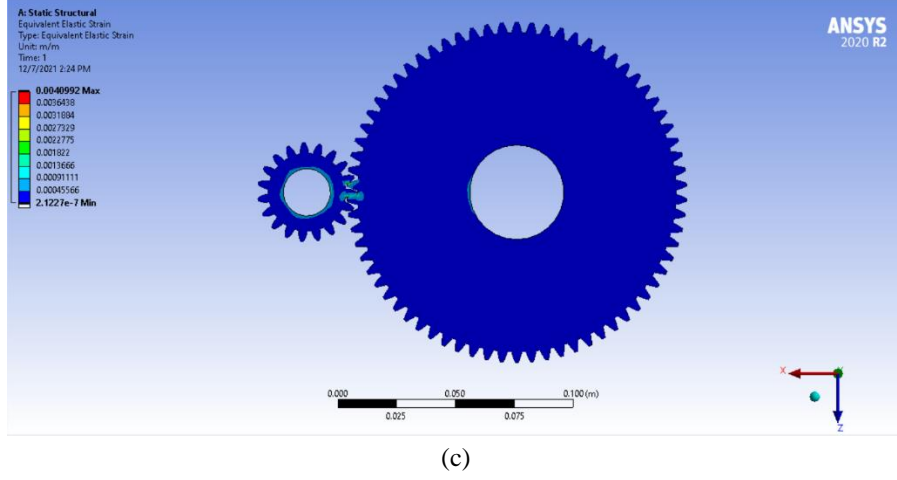
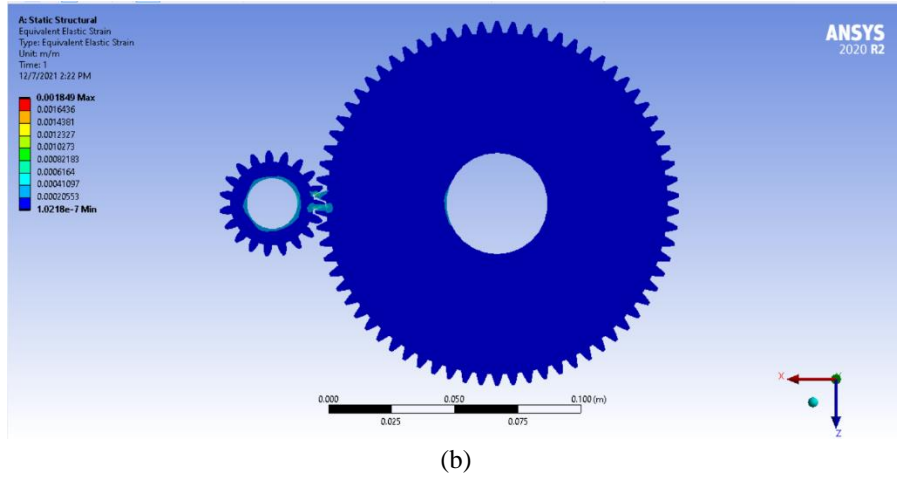
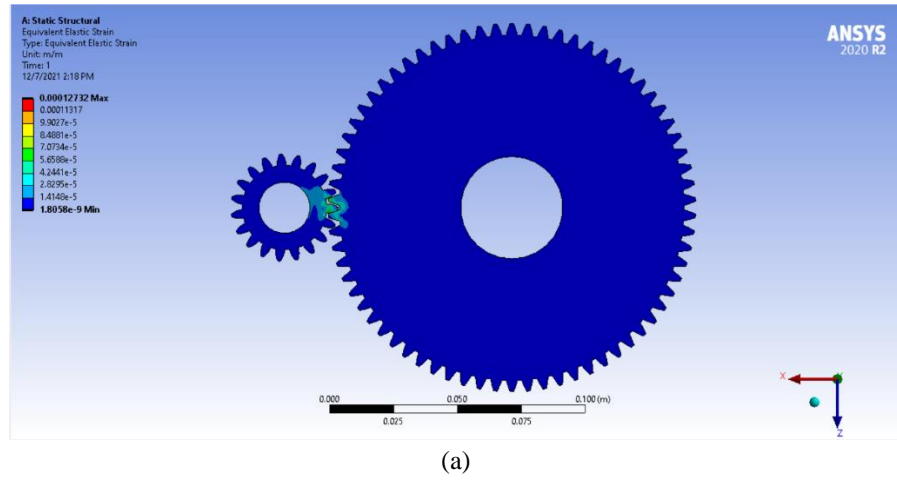


Figure (22): Equivalent elastic strain at. (a)22°C, (b)30°C, (c)40°C.

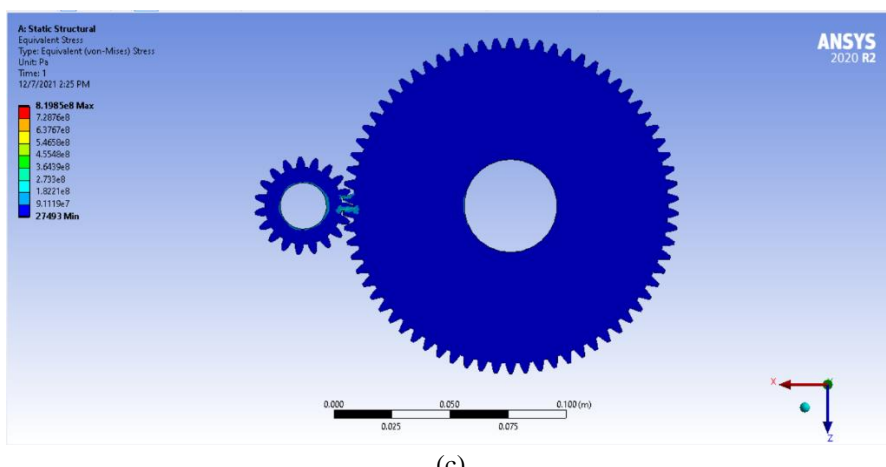
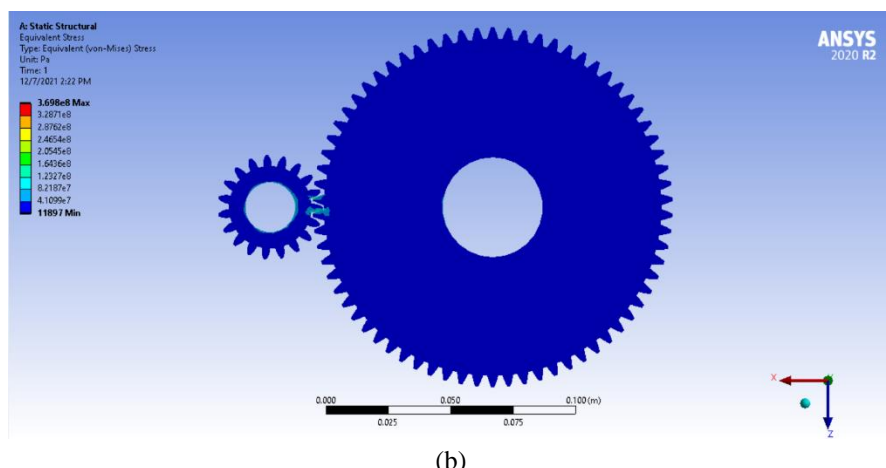
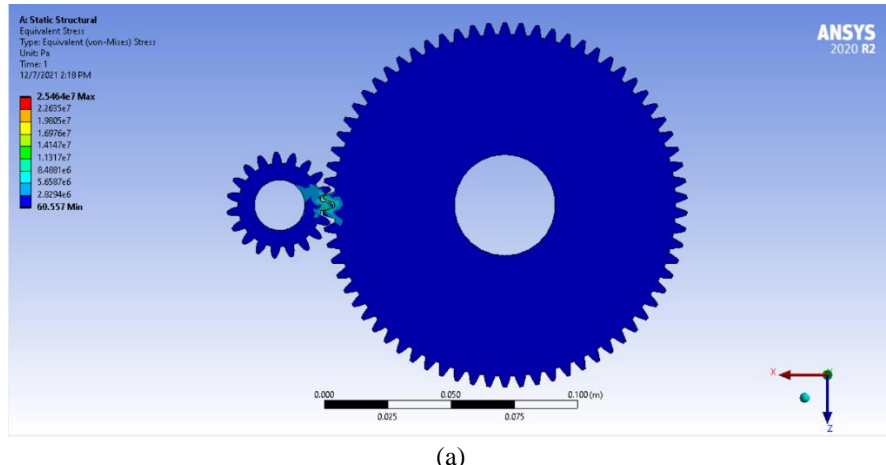


Figure (23): Equivalent stress at. (a)22°C, (b)30°C, (c)40°C.

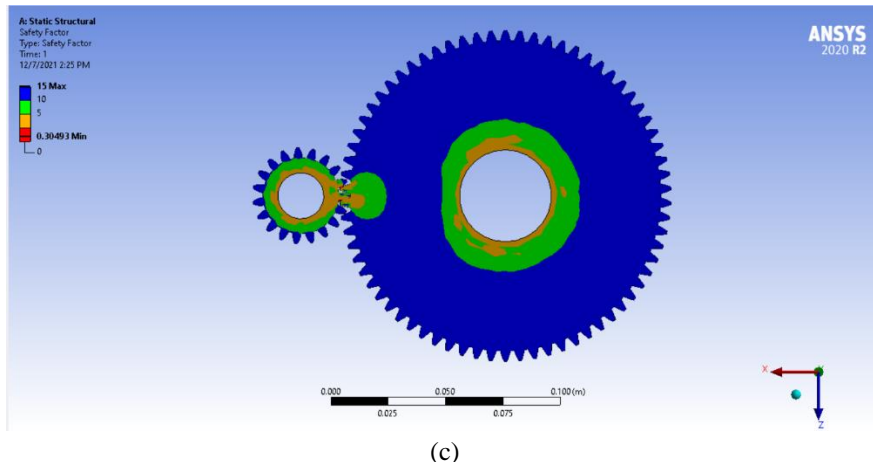
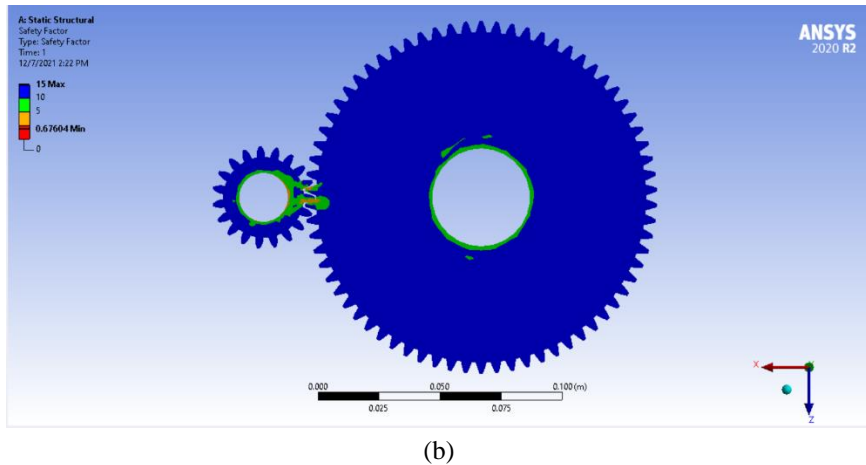
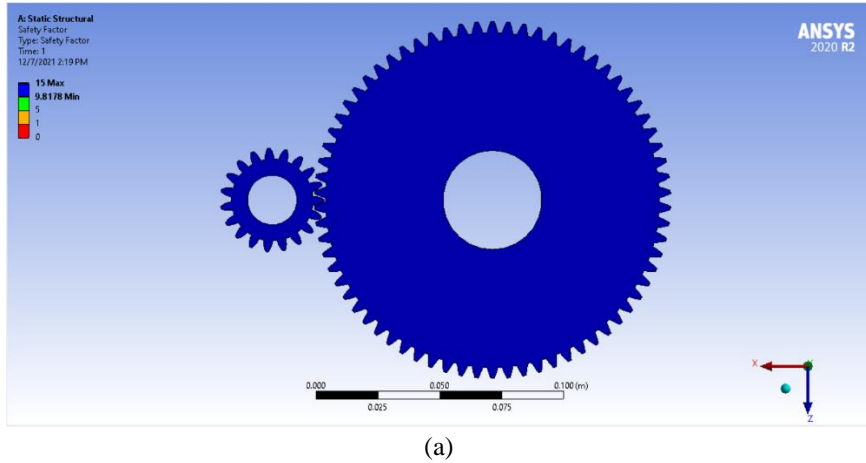


Figure (24): Safety factor at. (a)22°C, (b)30°C, (c)40°C.

Through the previous figures, we note the change and the clear effect of temperatures on the mechanical stresses of the gear, as it was found through the results of deformations that the higher the temperature, the greater the distortion that occurred in the gear, where the maximum distortion occurred at the temperature of 40 degrees Celsius 0.000014296m. We also note the clear difference in the effect of degrees The heat on the strain, where the largest value of the strain at the temperature 40 degrees Celsius was 0.0040992 m/m and since the strain increased as well as the deformation, the stress must increase with the increase in temperature, as it was at the temperature 40 degrees 819850000 pa. It is worth noting that the most important element is taken into consideration It is the constant of safety, as we clearly notice a decrease in the constant of safety with increasing temperatures, as it reached at the temperature of 40 degrees Celsius to 0.3 in some delicate areas of the teeth.

5. Conclusion

The study of the effect of heat on mechanical stress is essential to the operation of the tracking system in the solar collector, and it is necessary to understand and analyze all conditions that occur on these mechanical parts. A, where the upper and lower gear of the tracking system in the solar collector responsible for the movement of the solar collector horizontally and vertically, and the

stresses coming from the stepping motor with a torque of 8.5n/m in addition to the thermal stresses were studied. The results showed that with increasing temperatures, the mechanical stresses of the active parts increased, where the highest temperature of 40 degrees Celsius represented the strongest effect on the mechanical stresses. Where the deformation was 0.000014296m and the strain at this temperature reached 0.00409 m/m and the value of the stresses It reached great values due to the high temperature on the gear, reaching 819.850000Pa.Also, the safety factor was significantly and significantly reduced, reaching 0.3049, which is a very low value.

6. References

1. Saqer Ibrahim Al Ali, Jeremy (Zheng) Li. "Computed Aided Design and Simulation of a Dual Axis Sun Tracking Solar Panel Transmission." *International Journal of Applied Science and Technology*, vol. 7, no. 4, 2017. Accessed 1 Dec. 2021.
2. Dolara, Alberto; Grimaccia, Francesco; Leva, Sonia; Mussetta, Marco; Faranda, Roberto; Gualdoni, Moris (2012). *Performance Analysis of a Single-Axis Tracking PV System*. *IEEE Journal of Photovoltaics*, 2(4), 524–531. doi:10.1109/JPHOTOV.2012.2202876
3. Li, Gui Hua; Tang, Run Sheng; Zhong, Hao (2012). *Optical Performance of Horizontal Single-Axis Tracked Solar Panels*. *Advanced Materials Research*, 424-425(), 805–810. doi:10.4028/www.scientific.net/amr.424-425.805
4. C.S. Chin; A. Babu; W. McBride (2011). *Design, modeling and testing of a standalone single axis active solar tracker using MATLAB/Simulink*. , 36(11), 3075–3090. doi:10.1016/j.renene.2011.03.026
5. Kabalci, Ersan; Calpbincici, Ayberk; Kabalci, Yasin (2015). [*IEEE 2015 7th International Conference on Electronics, Computers and Artificial Intelligence (ECAI) - Bucharest, Romania (2015.6.25-2015.6.27)*] *2015 7th International Conference on Electronics, Computers and Artificial Intelligence (ECAI) - A single-axis solar tracking system and monitoring software*. , (), SG-17–SG-22. doi:10.1109/ECAI.2015.7301193
6. Safan, Yasser M.; Shaaban, S.; Abu El-Sebah, Mohamed I. (2018). *Performance evaluation of a multi-degree of freedom hybrid controlled dual axis solar tracking system*. *Solar Energy*, 170(), 576–585. doi:10.1016/j.solener.2018.06.011
7. Alexandru, C; Pozna, C (2010). *Simulation of a dual-axis solar tracker for improving the performance of a photovoltaic panel*. *Proceedings of the Institution of Mechanical Engineers, Part A: Journal of Power and Energy*, 224(6), 797–811. doi:10.1243/09576509jpe871
8. Zhang, Peng; Zhou, Gongbo; Zhu, Zhencai; Li, Wei; Cai, Zhixiong (2013). *Numerical study on the properties of an active sun tracker for solar streetlight*. *Mechatronics*, 23(8), 1215–1222. doi:10.1016/j.mechatronics.2013.08.007
9. Mokhtari, B.; Ameur, A.; Mokrani, L.; Azoui, B.; Benkhoris, M. F. (2009). [*IEEE IECON 2009 - 35th Annual Conference of IEEE Industrial Electronics (IECON) - Porto, Portugal (2009.11.3-2009.11.5)*] *2009 35th Annual Conference of IEEE Industrial Electronics - DTC applied to optimize solar panel efficiency*. , (0), 1122–1127. doi:10.1109/iecon.2009.5414681